HNUE JOURNAL OF SCIENCE
Natural Sciences 2024, Volume 69, Issue 2, pp. 47-57
This paper is available online at http://hnuejs.edu.vn/ns
DOI: 10.18173/2354-1059.2024-0019

ALL-OPTICAL LOGIC GATE OPERATION WITH A MULTI-CORE NONLINEAR PHOTONIC CRYSTAL FIBER

Nguyen Dang Quang Huy[1], Tran Phuong Yen[1], Do Duc Tho[2], Cao Xuan Thang[3], Bui Duc Tinh[1], Tran Ky Vi[1], Mattia Longobucco[4,5], Nguyen Thi Dung[6], Tran Thi Hai[6] and Nguyen Viet Hung[3,*]

[1]*Faculty of Physics, Hanoi National University of Education, Hanoi city, Vietnam*
[2]*Faculty of Engineering Physics, Hanoi University of Science and Technology, Hanoi city, Vietnam*
[3]*School of Materials Science and Engineering, Hanoi University of Science and Technology, Hanoi city, Vietnam*
[4]*Łukasiewicz Research Network - Institute of Microelectronics and Photonics, Warsaw city, Poland*
[5]*School of Electrical and Electronics Engineering, Nanyang Technological University, 50 Nanyang Avenue, 639798, Singapore*
[6]*Department of Natural Sciences, Hong Duc University, Thanh Hoa city, Vietnam*
[*]Corresponding author: Nguyen Viet Hung, e-mail: hung.nguyenviet@itims.edu.vn

Received June 3, 2024. Revised June 19, 2024. Accepted June 26, 2024.

Abstract. In this paper, we propose the design of a photonic crystal fiber with four central cores infiltrated by a high-index liquid to achieve highly efficient control of light guidance. We analyze the field distribution, effective mode area, and dispersion characteristics of the fundamental guided modes of the fiber. Within the coupled-mode theory, the pulse propagation in the fiber is governed by coupled nonlinear Schrödinger equations. We use the split-step Fourier method to simulate the propagation of pulses numerically. The results show three features of the dynamics: oscillation, switching, and self-trapping. We predict that the fiber could operate as a logic-gate device by introducing suitable input and control signals.

Keywords: coupled nonlinear Schrodinger equations, logic gates, photonic crystal fiber, split-step Fourier algorithm.

1. Introduction

Electronic devices are becoming increasingly diverse and ubiquitous, playing a vital role in modern life. However, electronic components that use electrical signals have

drawbacks, including limited capacity and processing speed, as well as significant heat generation and energy loss. To overcome these shortcomings, there is a current focus on developing alternative technologies and materials to construct new types of devices, such as plasmonics [1] and metamaterials [2]-[3]. Photonic devices, which use optical signals to process and manipulate information [4], can also be considered a promising alternative, e.g., waveguides [5], switches [6], bistable devices [7], and logic gates [8]-[11]. Among these, photonic-crystal-based devices [12]-[14] are crucial functional components for integrated photonics, enabled by significant advances in micro- and nanoscale technologies over the last few decades.

Photonic crystal fiber represents one of the next generations of optical waveguides that can improve the efficient transmission of optical signals [15]. This innovative fiber features a core with periodically arranged dielectric structures that form a photonic crystal lattice. The fiber's central region can be either hollow core or solid core, with hollow core fibers using the photonic bandgap principle for waveguiding and solid core fibers using the total internal reflection principle [16]. Key applications of this new type of optical fiber include coupling [17], switching, and logic gates [18]-[20] in integrated photonic circuits.

In recent years, the field of opto-fluidics has developed rapidly with advances in materials science and nanotechnology [21]. This field is applied to the fabrication of new photonic crystal fibers, where liquid solutions of high refractive index (such as toluene, chloroform, ethylene glycol, benzene, etc.) are used to fill some of the central cores of the fiber to confine and control light waves. This technology enables the creation of multi-core photonic crystal fibers with novel dispersion characteristics that effectively perform certain signal processing functions for integrated circuits. In these fibers, complex localized structure modes are deeply rooted in the cores when suitable fluids are chosen. As a result, the nonlinear properties of the fiber become more pronounced, significantly affecting signal propagation. With these new properties of the multicore photonic crystal fibers, we expect to use them as components for implementing optical logic gates.

In this paper, we propose a new design of photonic crystal fiber that can effectively operate as an all-logic-gate device by applying the opto-fluidics technique. We will use toluene as a high-index material to fill four guided cores of the fiber. By changing the characteristics of the input signal pulses (pulse width, amplitude, phase, etc.), we can control both signal propagation and energy transfer between the fiber cores. Furthermore, by selecting the core positions for pulse illumination and using one of the cores as a control core, we can effectively regulate the signal transmission process. With four cores, the increased variety of choices for the two control signals and two input pulses enhances our chances of successfully implementing all the basic logic gates using the fiber.

2. Content

2.1. The fiber design and properties of guided modes

In this section, we propose a design of a photonic crystal fiber made of pure silica (SiO_2) as the background material, with circular air holes arranged in a triangular lattice. We filled the four holes around the central air hole with liquid toluene, which acts as the guiding core due to its higher refractive index compared to silica. This fiber structure can be implemented using Lumerical software [22] and is illustrated in Figure 1.

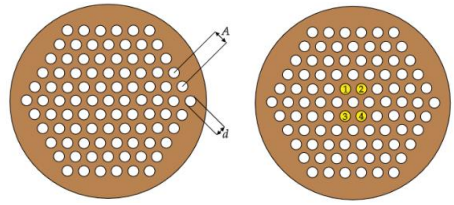

Figure 1. Design of the four-core photonic crystal fiber for optical logic-gate operation. The cores indexed by numbers 1 - 4 in the left panel are the guided cores of the fiber

In Figure 1, the cladding region SiO_2 is indicated in brown, the white circles represent the air holes, and the four guiding cores infiltrated by toluene are shown in yellow. The parameters of our fiber include the air hole diameter (d), pitch constant (A) with ratio $d / A = 0.666$. We set the pitch constant $A = 2$ μm and the size of the cladding to 20 μm. In order to analyze the mode structure of the fiber using the mode solver, we need to provide information about the refractive index of optical materials [23]-[26]. For pure silica, the index is determined by the Sellmeier equation [23]

$$n^2 = 1 + \frac{B_1\lambda^2}{\lambda^2 - C_1} + \frac{B_2\lambda^2}{\lambda^2 - C_2} + \frac{B_3\lambda^2}{\lambda^2 - C_3}, \tag{1}$$

while the Cauchy formula is used to calculate the index of toluene [24]-[25]

$$n^2 = B_0 + \frac{B_1}{\lambda^2} + \frac{B_2}{\lambda^4}, \tag{2}$$

The constants B_i in equations (1)-(2) can be estimated from experiment measurements, and their values are given in Table 1.

Table 1. The Cauchy and Sellmeier constants of toluene and pure silica

Toluene	B_0		B_1 (10^3 nm^2)		B_2 (10^8 nm^2)	
	1.474775		6.99031		2.1776	
Silica	B_1	B_2	B_3	C_1 (10^3 nm^2)	C_2 (10^3 nm^2)	C_3 (10^6 nm^2)
	0.69617	0.40794	0.89748	4.6791	13.512	97.934

In numerical calculations, the solver uses the provided refractive index of materials from (1) - (2) within a range of wavelengths between 1.3 μm and 1.6 μm to construct the guided modes of the fiber. For pulse propagation investigation, we focus on the properties of the fiber at the particular wavelength λ = 1.55 μm, which is commonly used in optical communication.

The electric field of the guiding modes can be represented as

$$\mathbf{E}(x, y, z, t) = \tilde{\mathbf{E}}(x, y).\exp(-\mathrm{i}\beta z + \mathrm{i}\omega t), \tag{3}$$

where ω is the mode frequency, $\tilde{\mathbf{E}}(x, y)$ is a spatial profile in the Oxy plane and β is the propagation constant along the guided z axis. From the Maxwell equations, we derive the Helmholtz equation for the electric field of guided mode as [5]

$$\frac{\partial\tilde{\mathbf{E}}}{\partial x^2} + \frac{\partial\tilde{\mathbf{E}}}{\partial y^2} + \left(\frac{n^2\omega^2}{c^2} - \beta^2\right)\tilde{\mathbf{E}} = 0, \tag{4}$$

where c is the speed of light in a vacuum. The numerical solver extracts the mode profile $\tilde{\mathbf{E}}(x, y)$ and the corresponding propagation constant β from the eigenvalue problem (4) at different wavelengths λ. This numerical data enables us to analyze the dispersive characteristics of the fiber. The dispersion parameter D of the mode is defined as [5]

$$D = -\frac{\lambda}{c}\frac{d^2 n_{eff}}{d\lambda^2}, \tag{5}$$

where the effective index is determined by $n_{eff} = \frac{\beta\lambda}{2\pi}$. The second order dispersion coefficient is [5]

$$\beta_2 = -\frac{\lambda^2}{2\pi c} D, \tag{6}$$

The results of the numerical calculations for the mode profiles are shown in Figure 2 for the four lowest localized modes. The field distribution of these modes is concentrated in the four toluene-filled cores, indicating that the optical energy is confined there. These are the so-called guiding modes in the fiber. We classify the modes into two pairs, with polarizations along the Ox (horizontal) and Oy (vertical) axes. The field distribution of the two modes in each pair can be symmetric or anti-symmetric. The pairs of modes with symmetric/anti-symmetric field profiles have similar propagation constant values. The anti-symmetric modes have larger propagation constants than the symmetric ones.

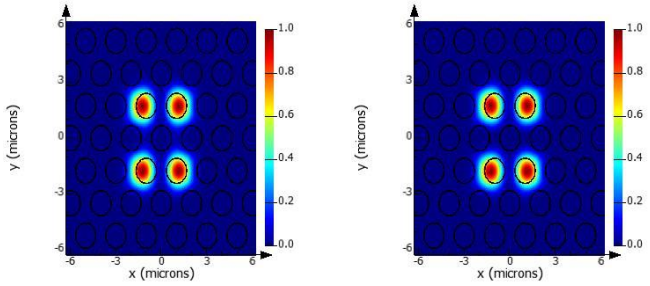

(*a) Horizontal X-polarization modes (left: symmetric, right: anti-symmetric)*

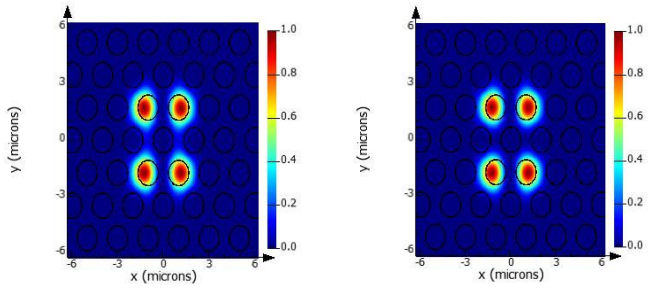

(b) Vertical Y-polarization modes (left: symmetric, right: anti-symmetric)

Figure 2. The four lowest guided modes in the four-core photonic crystal fiber

The dispersive characteristics D of the localized guided modes are presented in Figure 3. We observe normal dispersion for all modes. The dispersion of the antisymmetric modes increases consistently with respect to wavelength, while the

dispersion of the symmetric modes increases in the range of 1.3 μm to 1.45 μm and then decreases.

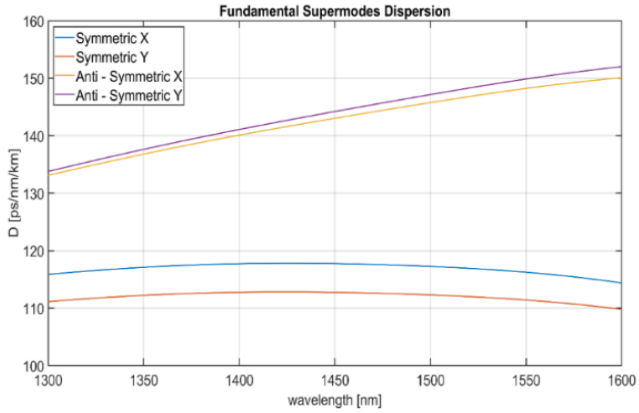

Figure 3. Dispersion characteristics of guided modes in the four-core photonic crystal fiber

We also calculate the effective mode area of the guided modes by using the formula [5]

$$A_{eff} = \frac{\left(\int\int_{-\infty}^{\infty} \left|\tilde{\mathbf{E}}(x,y)\right|^2 \mathrm{d}x\mathrm{d}y \right)^2}{\int\int_{-\infty}^{\infty} \left|\tilde{\mathbf{E}}(x,y)\right|^4 \mathrm{d}x\mathrm{d}y} \tag{7}$$

and used this quantity to determine the nonlinear parameter corresponding to the guided modes as

$$\gamma = \frac{2\pi n_2}{\lambda A_{eff}} \tag{8}$$

Here n_2 is the nonlinear refractive index of the toluene [24]-[26]. The result of calculations for nonlinear parameters of four guided modes is represented in Figure 4.

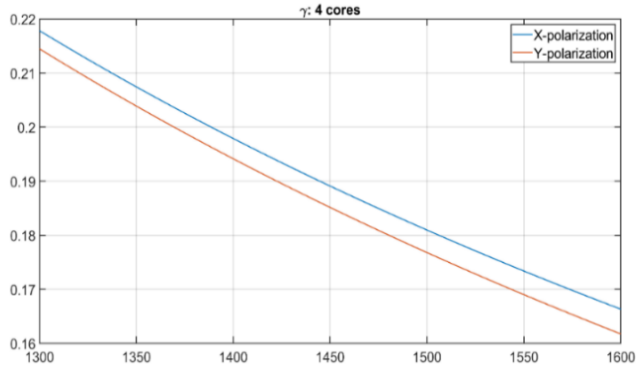

Figure 4. Nonlinear parameter of guided modes as a function of wavelength

We conclude that the pair of modes with horizontal polarization have the same nonlinear parameter. The modes with vertical polarization also have the same nonlinear parameter. This quantity decreases with the increase in wavelength. The nonlinear parameter of the horizontal modes is slightly larger than that of the vertical modes.

2.2. Nonlinear propagation of short pulse in the fiber and application

In this section, we investigate the nonlinear propagation of short optical pulses in the designed photonic crystal fiber to create all-optical logic gates. As seen in the study of the fundamental properties of guided modes in the previous section, the field of the modes predominantly occupies the toluene cores. This fact allows us to simplify the dynamics of pulse propagation in the fiber using coupled-mode theory. We can model the four-core photonic crystal fiber as a system of four coupled single-core fibers. The coupling between the single-core fibers is characterized by the coupling parameter as

$$\kappa_{pq} = \frac{\omega\varepsilon_0 \int\int_{-\infty}^{\infty} \left(n^2 - n_q^2\right) \tilde{\mathbf{E}}_p^* \tilde{\mathbf{E}}_q \mathrm{d}x\mathrm{d}y}{\int\int_{-\infty}^{\infty} \mathbf{u}_z \left(\tilde{\mathbf{E}}_p^* \times \tilde{\mathbf{H}}_p + \tilde{\mathbf{E}}_p \times \tilde{\mathbf{H}}_p^*\right) \mathrm{d}x\mathrm{d}y} \tag{9}$$

where p, q runs from 1 to 4 [5]. Here n is the refractive index profile of the fiber, n_q is the refractive index of the fiber when only the qth core among 4 guiding cores is infiltrated by toluene, $\tilde{\mathbf{E}}_{p,q}$ and $\tilde{\mathbf{H}}_{p,q}$ denote the electric and magnetic fields of the guided modes when either only the pth or qth guided core is filled by toluene. Due to the symmetry of the design of the fiber, we have $\kappa_{pq} = \kappa_{qp}$. Within the coupled-mode theory, the model of pulse propagation in the four-core photonic crystal fiber is based on the system of linearly coupled nonlinear Schrodinger equations (NLSEs), written for the electromagnetic envelope wavefunction $A_j(t,z)$ in each core as follows [5]:

$$\mathrm{i}\frac{\partial A_1}{\partial z} - \frac{\beta_2}{2}\frac{\partial^2 A_1}{\partial t} + \gamma\left|A_1\right|^2 A_1 + \kappa_{12}A_2 + \kappa_{13}A_3 + \kappa_{14}A_4 = 0 \tag{10 a}$$

$$\mathrm{i}\frac{\partial A_2}{\partial z} - \frac{\beta_2}{2}\frac{\partial^2 A_2}{\partial t} + \gamma\left|A_2\right|^2 A_2 + \kappa_{12}A_1 + \kappa_{14}A_3 + \kappa_{13}A_4 = 0 \tag{10 b}$$

$$\mathrm{i}\frac{\partial A_3}{\partial z} - \frac{\beta_2}{2}\frac{\partial^2 A_3}{\partial t} + \gamma\left|A_3\right|^2 A_3 + \kappa_{12}A_4 + \kappa_{14}A_1 + \kappa_{13}A_2 = 0 \tag{10 c}$$

$$\mathrm{i}\frac{\partial A_4}{\partial z} - \frac{\beta_2}{2}\frac{\partial^2 A_4}{\partial t} + \gamma\left|A_4\right|^2 A_4 + \kappa_{12}A_3 + \kappa_{14}A_2 + \kappa_{13}A_1 = 0 \tag{10 d}$$

where (z, t) are the propagation distance and time. The physical parameters $\beta_2, \gamma, \kappa_{12,13,14}$ represent the group-velocity dispersion (GVD), the Kerr nonlinearity, and the inter-core coupling, respectively. The values of these quantities at the wavelength λ = 1.55 μm are extracted from numerical data using the formulae (6), (8), (9) and shown in Table 2.

Table 2. The parameters used in the propagation simulation were calculated by Lumerical solver

Physical quantity	Value	Unit
β_2	-1.0132 10^{-25}	s^2/m
γ	0.563552	$1/(W.m)$
κ_{12}	42213.71	$1/m$
κ_{13}	729.82	$1/m$
κ_{14}	1826.4	$1/m$

In the numerical simulation, we used rescaled parameters $t = \sqrt{|\beta_2| / \kappa_{12}}\,\tau$, $z = \zeta / \kappa_{12}$, $A_i = \psi_i \sqrt{\kappa_{12} / \gamma}$ to convert the set of equations (10 a) - (10 d) to the dimensionless form

$$\mathrm{i}\frac{\partial \psi_1}{\partial \zeta} + \frac{1}{2}\frac{\partial^2 \psi_1}{\partial \tau^2} + |\psi_1|^2 \psi_1 + \left(\psi_2 + \frac{\kappa_{13}}{\kappa_{12}}\psi_3 + \frac{\kappa_{14}}{\kappa_{12}}\psi_4\right) = 0 \tag{11 a}$$

$$\mathrm{i}\frac{\partial \psi_2}{\partial \zeta} + \frac{1}{2}\frac{\partial^2 \psi_2}{\partial \tau^2} + |\psi_2|^2 \psi_2 + \left(\psi_1 + \frac{\kappa_{13}}{\kappa_{12}}\psi_4 + \frac{\kappa_{14}}{\kappa_{12}}\psi_3\right) = 0 \tag{11 b}$$

$$\mathrm{i}\frac{\partial \psi_3}{\partial \zeta} + \frac{1}{2}\frac{\partial^2 \psi_3}{\partial \tau^2} + |\psi_3|^2 \psi_3 + \left(\psi_4 + \frac{\kappa_{13}}{\kappa_{12}}\psi_1 + \frac{\kappa_{14}}{\kappa_{12}}\psi_2\right) = 0 \tag{11 c}$$

$$\mathrm{i}\frac{\partial \psi_4}{\partial \zeta} + \frac{1}{2}\frac{\partial^2 \psi_4}{\partial \tau^2} + |\psi_4|^2 \psi_4 + \left(\psi_3 + \frac{\kappa_{13}}{\kappa_{12}}\psi_2 + \frac{\kappa_{14}}{\kappa_{12}}\psi_1\right) = 0 \tag{11 d}$$

We use the standard split-step Fourier method [5] to simulate the propagation of pulses in the fiber. The initial pulses launched into the guided cores are assumed to be in Gaussian form as follows:

$$\psi_j(0,\tau) = a_j \exp\left(-\frac{\tau^2}{W_j^2}\right)\exp\left(\mathrm{i}\Delta\phi_j\right), \tag{12}$$

where a_j is amplitude, W_j indicates pulse duration and $\Delta\phi_j$ stands for the phase of each initial pulse. The energies of pulses are calculated by performing the integrations $\int_{-\infty}^{\infty} |\psi_i(0,\tau)|^2 \,\mathrm{d}\tau$.

The results of numerical simulations of the nonlinear propagation of pulses are shown in Figure 5. Here, we launched four Gaussian pulses with different initial amplitudes into the guided cores and investigated the dynamics of propagation using equations (11 a) - (11 d). In all simulations, we set the phases equal to zero and the pulse durations to 150 fs. Depending on the values of the initial amplitudes, we can classify three main features of the dynamics: oscillation, switching, and trapping phenomena.

In Figure 5a, when all of the amplitudes are small, $a_1 = 0.5$, $a_2 = 0.1$, $a_3 = 0.3$, and $a_4 = 0.1$, we see the periodic exchange of energies between the two pairs of cores 1 - 2 and 3 - 4. This occurs when the focusing nonlinear effect is weaker than dispersion and coupling; therefore, the pulses undergo tunneling and expansion during propagation.

When we increase at least one of the initial amplitudes, the periodic oscillation of energies breaks down. Figure 5b shows a typical example of this case with $a_1 = 1.55$, $a_2 = 0$, $a_3 = 0.5$, and $a_4 = 0.1$. Here, the exchange of energies in cores 1-2 is no longer periodic, and the energies tend to equalize to stable populations.

Continuing the simulation with larger values of one amplitude, we observe optical switching. At high enough energy, when the impact of the nonlinear effect is comparable to dispersion, the dynamics become sensitive to the initial states, and we can see the irreversible transfer of a large amount of pulse energy from one core to another during

propagation. Figure 5c illustrates this interesting phenomenon with $a_1 = 1.9$, $a_2 = 0$, $a_3 = 0.5$, and $a_4 = 0.1$.

A self-trapping effect appears if the amplitude a1a_1a1 reaches a higher value. In this situation, the focusing nonlinearity dominates the dispersion, causing the input pulse to localize in the initial core without transferring to other cores. In Figure 5d, we show the simulation with $a_1 = 1.95$, $a_2 = 0$, $a_3 = 0.5$, and $a_4 = 0.1$, where the self-trapping occurs.

We conducted simulations varying the relative phase of initial pulses and concluded that the relative phase significantly impacts the dynamics of optical switching and self-trapping.

The conclusions drawn from the numerical simulations above suggest that the designed photonic crystal fiber can be used for optical logic-gate operations. Similar to the procedure of calculations presented in Refs. [8]-[9], we determine the extinction ratio as follows:

$$XR(\mathrm{dB}) = 10.\mathrm{Log}_{10}\left(\frac{\int_{-\infty}^{\infty}\left|\psi_i(L,\tau)\right|^2 \mathrm{d}\tau}{\int_{-\infty}^{\infty}\left|\psi_j(L,\tau)\right|^2 \mathrm{d}\tau}\right) \tag{13}$$

with ψ_i and ψ_j are the fields of output signals, and L is the length of the fiber. For constructing optical logic gates, the control signals (CS) are launched into core 1 and core 4 while the input signals *(I_1;* and *I_2)* are provided through core 2 and core 3. By choosing appropriate amplitudes and relative phases of the CSs, we can obtain the expected output signals *(O_1; O_2)*, which are suitable for desired logic gates.

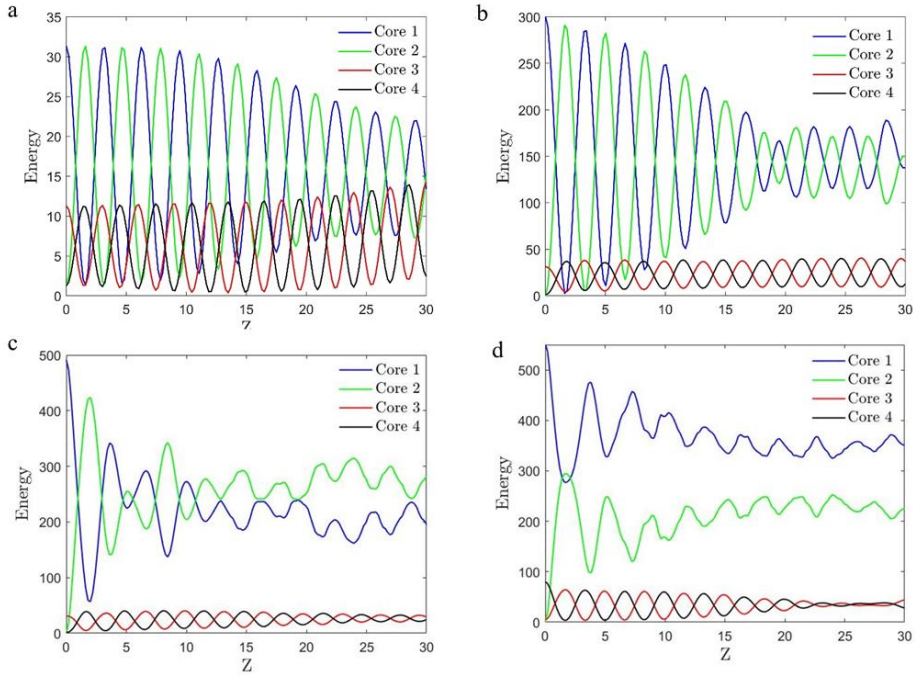

Figure 5. The dynamics of pulse propagation with different regimes of initial amplitudes, showing the oscillation, switching, and trapping effects

In Tables 3 and 4, we summarize the results from systematic numerical calculations for the extinction ratios XR_1 and XR_2 of the output at core 2 and core 3 in various cases of different phases and amplitudes of the control signals in core 1 and core 4. Here, we applied the inputs $(I_1; I_2)$ with a set of signals (0;0); (0;1) (1;0), and (1;1) and determined the corresponding output $(O_1; O_2)$ based on the rules in which the positive value of XR indicates the output 1 while a negative value indicates the output 0. By launching the control signals into cores 1 and 4 with tunable relative phases between them, we can construct the truth tables for all fundamental logical gates. Table 3 presents the truth tables of the XNOR, XOR, NOR, and OR gates while Table 4 shows the truth tables for the AND, NAND, and NOT gates.

Table 3. Truth tables of the XNOR, XOR, NOR, and OR logic gates using the designed fiber. The control signals are given in the core 1 and 4 with different relative phases

Inputs		$\Delta\phi_1 = \frac{2\pi}{5}; a_1 = 2.1; \Delta\phi_4 = \frac{13\pi}{10}; a_4 = 2.1$		$\Delta\phi_1 = \frac{13\pi}{10}; a_1 = 2; \Delta\phi_4 = \frac{3\pi}{5}; a_4 = 2$	
I_1	I_2	O_1	O_2	O_1	O_2
0	0	1 1.2495dB	0 -1.2495dB	1 1.287dB	0 -1.287dB
0	1	0 -2.1153dB	1 2.1153dB	0 -1.211dB	1 1.211dB
1	0	0 -0.4912dB	1 0.4912dB	0 -0.74dB	1 0.74dB
1	1	1 0.6585dB	0 -0.6585dB	0 -1.544dB	1 1.544dB
Gates		XNOR	XOR	NOR	OR

Table 4. Truth tables of the AND, NAND, NOT logic gates using the designed fiber. The control signals are given in the core 1 and 4 with different relative phases

Inputs		$\Delta\phi_1 = \frac{3\pi}{10}; a_1 = 2; \Delta\phi_4 = \pi; a_4 = 2$		$\Delta\phi_1 = \frac{\pi}{2}; a_1 = 2; \Delta\phi_4 = \pi; a_4 = 2$	
I_1	I_2	O_1	O_2	O_1	O_2
0	0	0 -0.3736dB	1 0.3736dB	0 -1.0895dB	1 1.0895dB
0	1	0 -1.9149dB	1 1.9149dB	1 0.4461dB	0 -0.4461dB
1	0	0 -0.6572dB	1 0.6572dB	0 -1.0279dB	1 1.0279dB
1	1	1 0.9190dB	0 -0.9190dB	1 0.2316dB	0 -0.2316dB
Gates		AND	NAND		NOT

3. Conclusions

In this study, we proposed a design of a photonic crystal fiber filled with high-index liquid toluene in four central cores for the light-guiding function. We analyzed important properties of its guided modes, such as field distribution, dispersion, and effective mode area, in detail. We then applied coupled-mode theory to investigate the nonlinear propagation of pulses through the fiber. The numerical simulations show three typical dynamics, including oscillation, switching, and self-trapping, depending on the relative phases and amplitudes of the input pulses. As we expected, the designed fiber can function as all the basic logic gates if the input and control signals are appropriately chosen. Another fiber design to implement all the logic gates will be realized in the next work, using a higher-order nonlinear optical material in the guided cores.

Acknowledgment. This research is supported by the Ministry of Education and Training, Vietnam (grant number B2022-BKA-14).

REFERENCES

[1] Maier SA, (2007). *Plasmonics: Fundamentals and Applications,* Springer.

[2] Vu DL, (2018). *Modified materials with negative refractive index.* Science and Technology Publishing House.

[3] Pham VD, Mai DT, Pham QT, Vu MT, Vu DL, Nguyen AD, Man HN & Tran MC, (2023). Multi-element unit cell metamaterial absorber for the GHz frequency applications. *HNUE Journal of Science,* 68(3), 35-42. DOI: 10.18173/2354-1059.2023-0058.

[4] Salech BEA & Teich MC, (2019). *Fundamentals of Photonics* (3rd ed.), Wiley & Sons.

[5] Agrawal GP, (2019). *Nonlinear fiber optics* (6th ed.), Academic Press.

[6] Nguyen VH, Le XTT, Mattia L, Ryszard B, Ignac B, Ignas A, Audrius P, Andrius B, Boris M & Marek T, (2023). Self-trapping and switching of solitonic pulses in mismatched dual-core highly nonlinear fibers. *Chaos, Solitons and Fractals,* 167, 113045. DOI: 10.1016/j.chaos.2022.113045.

[7] Hoang TT, Ngo QM, Vu DL & Nguyen PTH, (2018). Controlling Fano resonances in multilayer dielectric gratings towards optical bistable devices. *Scientific Reports* 8(1), 1-8. DOI: 10.1038/s41598-018-34787-9.

[8] Menezes JWM, de Fraga WB, Ferreira AC, Saboia KDA, Filho AFGF, Guimarães GF, Sousa JRR, Rocha HHB & Sombra ASB, (2007). Logic gates based in two- and three-modes nonlinear optical fiber couplers. *Optical and Quantum Electronics,* 39, 1191-1206. DOI: 10.1007/s11082-008-9186-9.

[9] Menezes JWM, de Fraga WB, Guimaraes GF, Ferreira AC, Rocha HHB, da Silva MG & Sombra ASB, (2007). Optical switches and all-fiber logical devices based on triangular and planar three-core nonlinear optical fiber couplers. *Optics Communications* 276, 107-115. DOI: 10.1016/j.optcom.2007.03.071.

[10] Fraga WB, Menezes JWM, da Silva MG, Sobrinho CS & Sombra ASB, (2006). All-optical logic gates based on an asymmetric nonlinear directional coupler. *Optics Communications* 262, 32-37. DOI: 10.1016/j.optcom.2005.12.033.

[11] Singh P, Tripathi DKr, Jaiswal S & Dixit HK, (2014). All-Optical Logic Gates: Designs, Classification, and Comparison. *Advances in Optical Technologies*, 275083. DOI: 10.1155/2014/275083.
[12] Joannopoulos JD, Johnson SG, Winn JN & Meade RD, (2008). *Photonic Crystals - Molding the flow of light* (2nd ed.), Princeton University Press.
[13] Parandin F, Malmir MR, (2020). Low Delay Time All Optical NAND, XNOR and OR Logic Gates Based on 2D Photonic Crystal Structure. *Journal of Electrical and Computer Engineering Innovations*, 8(1), 1-8. DOI: 10.22061/JECEI.2020.6809.342.
[14] Jandieri V, Khomeriki R, Onoprishvili T, Erni D, Chotorlishvili L, Werner DH & Berakdar J, (2021). Band-Gap Solitons in Nonlinear Photonic Crystal Waveguides and Their Application for Functional All-Optical Logic Gating. *Photonics*, 8, 250. DOI: 10.3390/photonics8070250.
[15] Poli F, Cucinotta A & Selleri S, (2007). *Photonic* crystal *fibers*, Springer.
[16] Buczynski R, (2004). Photonic crystal fibers. *Acta Physica Polonica A*, 106, 141-167. DOI: 10.12693/APhysPolA.106.141.
[17] Liu M, Chiang KS, (2010). Propagation of ultrashort pulses in a nonlinear two-core photonic crystal fiber. *Applied Physics B,* 98, 815-820. DOI: 10.1007/s00340-009-3870-8.
[18] Martins FLB, Rodrigues JPT, Neto FGM, Nascimento JC, Coelho Jr AG & Fraga WB, (2018). Two and three-input All-optical logic gates on a planar three-core photonic crystal fiber. *Optik* 154, 516-523. DOI: 10.1016/j.ijleo.2017.10.067.
[19] Coelho AG, Costa MBC, Ferreira AC, da Silva MG, Lyra ML & Sombra ASB, (2013). Realization of All-Optical Logic Gates in a Triangular Triple-Core Photonic Crystal Fiber. *Journal of Lightwave Technology* 31(5), 731-739. DOI: 10.1109/JLT.2012.2232641.
[20] Uthayakumar T, Vasantha Jayakantha Raja R, and Porsezian K, (2013). Realization of all-optical logic gates through three core photonic crystal fiber. *Optics Communications*, 296, 124-131. DOI: 10.1016/j.optcom.2012.12.061.
[21] Fainman Y, Psaltis D & Yang C, (2010). *Optofluidics: Fundamentals, Devices, and Applications*, The McGraw-Hill Companies, Inc.
[22] https://www.lumerical.com.
[23] Arif MFH, Biddut MJH, (2017). Enhancement of relative sensitivity of photonic crystal fiber with high birefringence and low confinement loss. *Optik*, 131, 697-704. DOI: 10.1016/j.ijleo.2016.11.203.
[24] Samoc A, (2003). Dispersion of refractive properties of solvents: Chloroform, toluene, benzene, and carbon disulfide in ultraviolet, visible, and near infrared. *Journal of Applied Physics*, 94(9), 6167-6174. DOI: 10.1063/1.1615294.
[25] El-Kashef H, (2000). The necessary requirements imposed on polar dielectric laser dye solvents. *Physica B*, 279, 295-301. DOI: 10.1016/S0921-4526(99)00856-X.
[26] Kedenburg S, Steinmann A, Hegenbarth R, Steinle T & Giessen H, (2014). Nonlinear refractive indices of nonlinear liquids: Wavelength dependence and influence of retarded response. *Applied Physics B*, 117, 803-816. DOI: 10.1007/s00340-014-5833-y.